

Structure–Activity Relationships | Hot Paper |

Efficient Biomimetic Hydroxylation Catalysis with a Bis(pyrazolyl)imidazolymethane Copper Peroxide Complex

Claudia Wilfer,^[a, b] Patricia Liebhäuser,^[b] Alexander Hoffmann,^[b] Hannes Erdmann,^[a] Oleg Grossmann,^[a] Leander Runtsch,^[a] Eva Paffenholz,^[b] Rahel Schepper,^[c] Regina Dick,^[c] Matthias Bauer,^[c] Maximilian Dürr,^[d] Ivana Ivanović-Burmazović,^[d] and Sonja Herres-Pawlis^{*[a, b]}

Dedicated to Prof. Dr. Heinz Decker on the occasion of his 65th birthday

Abstract: Bis(pyrazolyl)methane ligands are excellent components of model complexes used to investigate the activity of the enzyme tyrosinase. Combining the N donors 3-*tert*-butylpyrazole and 1-methylimidazole results in a ligand that is capable of stabilising a (μ - η^2 : η^2)-dicopper(II) core that resembles the active centre of tyrosinase. UV/Vis spectroscopy shows blueshifted UV bands in comparison to other known peroxo complexes, due to donor competition from different ligand substituents. This effect was investigated with the help of theoretical calculations, including DFT and natural transition orbital analysis. The peroxo complex acts as a cata-

lyst capable of hydroxylating a variety of phenols by using oxygen. Catalytic conversion with the non-biological phenolic substrate 8-hydroxyquinoline resulted in remarkable turnover numbers. In stoichiometric reactions, substrate-binding kinetics was observed and the intrinsic hydroxylation constant, k_{ox} , was determined for five phenolates. It was found to be the fastest hydroxylation model system determined so far, reaching almost biological activity. Furthermore, Hammett analysis proved the electrophilic character of the reaction. This sheds light on the subtle role of donor strength and its influence on hydroxylation activity.

Introduction

A major part of research in the field of bioinorganic chemistry revolves around the development of model complexes that imitate the catalytic centre of enzymes. With these, chemists investigate reaction mechanisms or recreate the catalytic reactions of enzymes.^[1]

Tyrosinase is a widespread enzyme in mammals, birds, plants and fungi.^[2] Comprising a dicopper(II) peroxide core, it

belongs to the class of type-III copper enzymes.^[3,4] In its active centre, each copper atom is surrounded by three histidine moieties.^[3]

Reactions catalysed by tyrosinase include the *ortho*-hydroxylation of phenols to catechols and subsequent oxidation to quinones.^[3–6] After X-ray crystallographic characterisation of *Streptomyces castaneoglobisporus* tyrosinase by Matoba et al. in 2006, it has been accepted that a (μ - η^2 : η^2)-dicopper(II) peroxide core is present in tyrosinase.^[3]

For the formation of the peroxide core in model chemistry, a copper(I) species is reacted with O₂. In general, this reaction can result in several products,^[4–6] but most frequently the (μ - η^2 : η^2)-peroxide copper(II) core (⁵P core) and the isomeric bis(μ -oxo)dicopper(III) core (O core) are found; these are nearly isoenergetic and exist in equilibrium at low temperatures.^[7–9] The steric properties and, more importantly, the basicity of the ligands used determine whether the ⁵P or the O core is generated preferably. Therefore, many ligand families have been investigated as building blocks of tyrosinase and related hemo-cyanin models, including tris(pyrazolyl)borates,^[10] tris(pyrazolyl)methanes,^[11] alkyl amines,^[12] pyridines,^[13,14] ketimines^[15] and guanidines.^[16,17] Changing the ligand class can result in the formation of another Cu₂O₂ species, but can also vary within a ligand class, for example, by changing one donating substituent. We have investigated donor competition between pyridinyl and pyrazolyl moieties in the HC(3-*t*BuPz)₂(Py) ligand (3-*t*BuPz = 3-*tert*-butylpyrazolyl, Py = pyridyl) and shown

[a] Dr. C. Wilfer, H. Erdmann, O. Grossmann, L. Runtsch, Prof. Dr. S. Herres-Pawlis

Department für Chemie und Pharmazie
Ludwig-Maximilians-Universität München
Butenandtstraße 5–13, 81377 München (Germany)

[b] Dr. C. Wilfer, P. Liebhäuser, Dr. A. Hoffmann, E. Paffenholz, Prof. Dr. S. Herres-Pawlis

Institut für Anorganische Chemie
Rheinisch-Westfälische Technische Hochschule Aachen
Landoltweg 1, 52074 Aachen (Germany)
E-mail: sonja.herres-pawlis@ac.rwth-aachen.de

[c] R. Schepper, R. Dick, Prof. Dr. M. Bauer
Department Chemie, Universität Paderborn
Warburger Straße 100, 33098 Paderborn (Germany)

[d] M. Dürr, Prof. Dr. I. Ivanović-Burmazović
Department Chemie und Pharmazie
Friedrich-Alexander-Universität Erlangen-Nürnberg
Egerlandstraße 1, 91058 Erlangen (Germany)

Supporting information for this article is available on the WWW under <http://dx.doi.org/10.1002/chem.201501685>.

that nucleophilicity and basicity have to be taken into account.^[18–20]

After the first examples of stoichiometric hydroxylations mediated by a peroxy species,^[21–23] few ligand systems have been able to achieve significant catalytic phenol hydroxylation so far. In 1990 Réglier et al. presented a model containing a

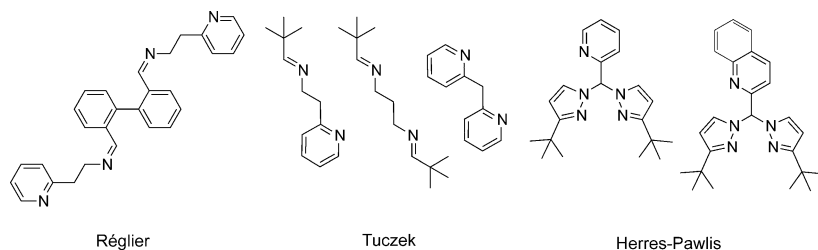


Figure 1. Ligands used for catalytic tyrosinase modelling.

biphenyl spacer (Figure 1).^[24] Casella et al. were later able to achieve the first monophenolase reaction by using a Cu_2O_2 complex.^[25] Since then, the group has made significant contributions concerning hydroxylation reactions in particular.^[26–29] In 2010, Tuczek et al. followed with a mononuclear copper(I) complex that consisted of pyridine and/or imine moieties as precursors (Figure 1).^[30] Recently, we presented the first room-temperature-stable, catalytic tyrosinase model that consisted of bis(pyrazolyl)methanes (Figure 1),^[31] whereas Tuczek et al. published catalytic systems with ligands that consisted of imine and benzimidazole and imine and pyrazolyl moieties, respectively.^[32,33] In the next step, they could prove that an auxiliary base, such as NEt_3 , was not always necessary for the conversion of phenolic substrates. Thereby, the phenol was attached to a pyridine-containing ligand and its proper positioning in close proximity to the copper dioxygen unit was sufficient to convert the phenol into an *ortho*-quinone.^[34] Lumb et al. made use of catalytic Cu/O_2 chemistry to generate valuable organic products from simple substituted phenols.^[35,36] They could also oxidise primary and secondary alcohols by using a tyrosinase mimic as a catalyst, which made the oxidising agent 2,2,6,6-tetramethylpiperidinyloxy (TEMPO) unnecessary.^[37]

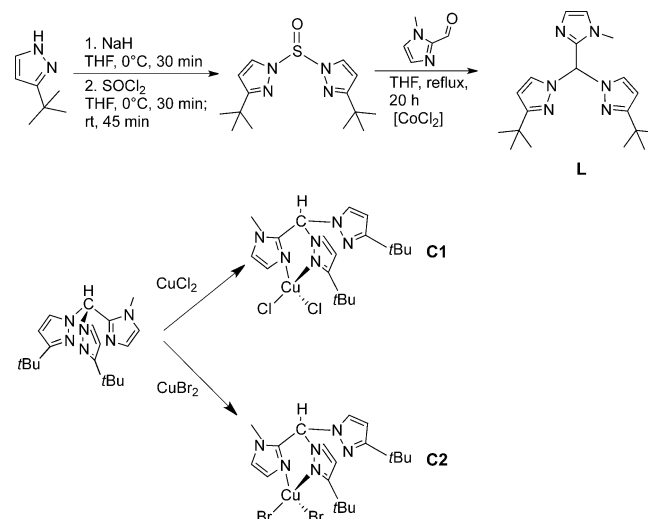
We developed a new bis(pyrazolyl)methane ligand as part of a functional tyrosinase model. In addition to catalytic studies, DFT and natural transition orbital (NTO) calculations were performed to further investigate the electronic structure of the complex and to gain an insight into electron transitions that occurred during the formation of the ^5P core.

By keeping the 3-*t*BuPz units because their bulky alkyl group prevents the formation of bisfacial complexes, pyridinyl was substituted by 1-methylimidazolyl (1-Melm; Scheme 1). The use of imidazolyl as a N-donating ligand is obvious because it is the key building block of the amino acid histidine.^[38] Thus, ligands containing imidazolyl moieties have already been applied in the field of copper-oxygen chemistry. In 1995, Sorrell et al. used a substituted tris(imidazolyl)phosphine ligand to stabilise a peroxy dicopper(II) adduct.^[39] Karlin and co-workers

followed in 2009 with an imidazolyl-containing tris(2-pyridylmethyl)amine (TMPA) derivative,^[40] and in 2012 Limberg et al. presented a tripodal ligand containing sterically demanding imidazolyl moieties for the stabilisation of Cu^{I} and Cu^{II} species.^[41] Those species were also capable of oxygen activation. Earlier this year, they demonstrated the hydroxylation of 2,4-di-*tert*-butylphenol (DTBP) to the

corresponding quinone with this system.^[42] In parallel, Stack et al. showed that a P species with simple methylimidazoles could be stabilised at extremely low temperatures of -120°C and also displayed hydroxylation activity.^[43]

Remarkably, these previous imidazolyl-containing systems did not show the catalytic activi-



Scheme 1. Synthesis of L, C1 and C2.

ty demonstrated herein with the novel bis(pyrazolyl)imidazolyl-methane ligand $\text{HC}(3\text{-}t\text{BuPz})_2(1\text{-Melm})$ (L).

Results and Discussion

Ligand and complex syntheses

Ligand L was prepared by using a synthetic procedure analogous to that reported previously (Scheme 1).^[44] The substituted pyrazole is deprotonated and treated with thionylchloride, resulting in the sulfoxide. In the following step, 1-methyl-2-imidazolecarboxaldehyde is added to the mixture and, under CoCl_2 catalysis and reflux conditions, the bis(pyrazolyl)methane ligand L is formed (Scheme 1 and Figure 2). Upon reaction of L with CuCl_2 , single crystals of $[\text{CuCl}_2\{\text{HC}(3\text{-}t\text{BuPz})_2(1\text{-Melm})\}]$ (C1) could be obtained from the reaction mixture. Furthermore, the reaction of CuBr_2 with L afforded single crystals of $[\text{CuBr}_2\{\text{HC}(3\text{-}t\text{BuPz})_2(1\text{-Melm})\}]\cdot\text{MeCN}$ (C2; Scheme 1 and Figure 2).

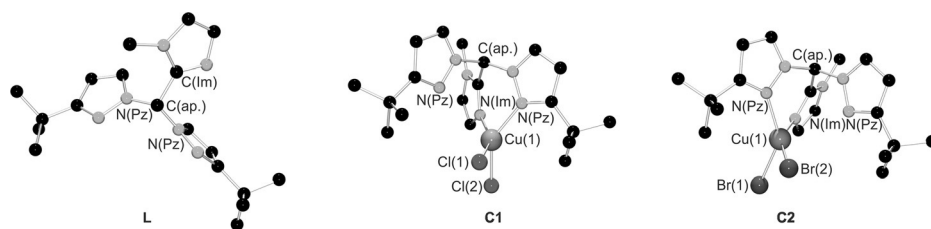


Figure 2. Molecular structures of L, C1 and C2.

Table 1. Selected experimental and calculated (Gaussian 09, TPSSh, 6-31g(d)) ^[51] bond lengths [Å] and angles [°] of L, C1 and C2.						
Bond lengths [Å]						
	L exptl		C1 exptl (X = Cl)	C1 calcd (X = Cl)	C2 exptl (X = Br)	C2 calcd (X = Br)
C _{ap} -N _{pz}	1.450(2) 1.451(2)	Cu-X(1)	2.225(1)	2.240	2.404(1)	2.316
C _{ap} -C _{im}	1.507(2)	Cu-X(2)	2.251(1)	2.218	2.353(1)	2.316
N _{pz} -N _{pz}	1.358(2) 1.367(2)	Cu-N _{pz}	2.044(3)	2.000	2.073(4)	2.036
		Cu-N _{im}	1.957(3)	1.961	1.964(4)	1.977
		C _{ap} -N _{pz}	1.455(4) 1.462(4)	1.457 1.459	1.467(5) 1.452(6)	1.461 1.456
		C _{ap} -C _{im}	1.502(5)	1.502	1.493(6)	1.501
Bond angles [°]						
N _{pz} -C _{ap} -N _{pz}	111.4(1)	X(1)-Cu-X(2)	97.3(1)	103.3	94.5(1)	102.6
N _{pz} -C _{ap} -C _{im}	109.9(1) 110.7(1)	X(1)-Cu-N _{pz}	98.8(1)	95.5	100.6(1)	93.9
		X(1)-Cu-N _{im}	150.8(1)	137.4	152.6(1)	144.6
		X(2)-Cu-N _{pz}	141.7(1)	146.8	142.0(1)	146.3
		X(2)-Cu-N _{im}	93.4(1)	94.8	93.5(1)	95.1
		N _{pz} -Cu-N _{im}	89.3(1)	89.3	88.9(2)	87.6
τ_4 ^[45]			0.48	0.54	0.46	0.49

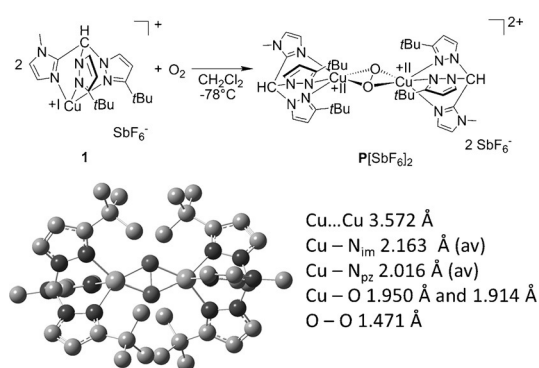
Table 1 displays key bond lengths and angles for the four-coordinate copper(II) complexes **C1** and **C2** and ligand **L** itself. Ligand **L** is a substituted methane and as such crystallises as an almost perfect tetrahedron in the triclinic space group $P\bar{1}$. Bond lengths are in the common range known for bis(pyrazolyl)methanes.^[44] In both molecular structures of **C1** and **C2**, one pyrazolyl moiety is pushed out of the coordination sphere around the copper atom, which suggests that the imidazolyl moiety has a stronger donor ability towards the central metal. The Cu-N_{im} bond length is shorter than the Cu-N_{pz} bond in **C1** and **C2**. The τ_4 values indicate a distorted coordination geometry, which can neither be assigned to a distorted tetrahedron nor to square-planar geometry.^[45] The Cu-N_{pz}, Cu-N_{im} and Cu-X bond lengths are shorter in **C1** than those in **C2**. Based on the molecular structures of **C1** and **C2**, we conducted DFT structural optimisations. The results are also displayed in Table 1. By comparing experimental and calculated bond lengths for **C1**, a proper accordance is found because the only bond length predicted to be too short is the Cu-Cl(2) one. For bond angles, the calculations show the same dispersion as in the molecular structure of **C1**. For example, the N_{pz}-Cu-N_{im} and Cl(2)-Cu-N_{im} angles are predicted almost correctly, whereas all others deviate by not more than 6°, excluding the Cl(1)-Cu-N_{im} angle. For **C2**, the calculated angles at the copper atom are

not as accurate as those for **C1**; however, the bond lengths are predicted well. Bond angles are predicted to be either too large or too small, but overall result in a predicted τ_4 value that is similar to the experimental one. With regard to possible conformers with tridentate or bis(pyrazolyl) coordination, we tried to obtain other conformer structures. It should be noted that all attempts failed and yielded the experimentally found conformers. However, the observed pyrazolyl-imidazolyl coordination is not caused by steric hindrance of the large *tert*-butyl groups, since we already have structurally characterised comparable copper(II) halide complexes with the sterically similar ligand HC(3-*t*BuPz)₂(Py).^[19] We interpret this finding as an indication of the slightly stronger donor strength of imidazolyl groups, as already discussed by others.^[46–48] Hence, compared with pyridinyl units, the imidazolyl unit is the strongest donor in the series Py < Pz < Im.^[46]

For a more detailed understanding of donation effects in complexes **C1**, **C2** and the peroxo complex **P**, which includes the ligand **L**, natural bond orbital (NBO) analysis was performed, yielding NBO charges and charge-transfer (CT) energies related to donation from the pyrazolyl and imidazolyl moieties to the copper atom. NBO charges are not absolute charges, but can help in the understanding of electronic effects in complexes.^[49–52] The NBO charges and CT energies are summarised in Table 2.

Table 2. NBO charges [e ⁻ units] and CT energies [kcal mol ⁻¹] for C1 , C2 and P . (Gaussian 09, TPSSh/6-31g(d) and NBO 6.0). ^[49–51]			
	C1	C2	P
NBO charges			
N _{im}	-0.57	-0.56	-0.61
N _{pz} (coord.)	-0.37	-0.36	-0.46
N _{pz}	-0.35	-0.30	-0.46
Cu	0.86	0.70	1.38
X(1)	-0.57	-0.48	
X(2)	-0.55	-0.48	
CT energies			
N _{im} →Cu	22.4	22.6	23.7/23.9
N _{pz} →Cu	21.1	19.9	36.8/38.6

The results in Table 2 reveal that N_{im} donor atoms possess a more negative charge than the N_{pz} donor atoms, and that the NBO charge at the non-coordinating N_{pz} atom is less negative than that on the coordinating one. However, the pK_a values and partial charges on the coordinating N atoms mostly do not give conclusive indications, as shown earlier.^[18,20] Analysis of the CT energies suggests a slightly larger donor ability of the nitrogen lone pair of imidazolyl to the central metal. This might be related to the shorter Cu– N_{im} bond length. For the P species, the NBO calculations show higher CT energies for pyrazolyl. This seems to be the case when the imidazolyl units are located at the axial positions, which lie at a slightly longer distance from the copper centre. This conformer (Scheme 2) was



Scheme 2. Top: Preparation of the side-on peroxide species P. Bottom: Calculated structure of the P species after geometry optimisation with TPSSH/6-31g(d).

used for all theoretical investigations because it was the energetically favourable one. Moreover, due to the mirror plane, the orbitals of this conformer appear more symmetrical and therefore clearer. We found that all possible conformers lay within 2 kcal mol⁻¹. In the other conformers, the CT energy also depends on the corresponding Cu–N distances, which makes analysis more complicated. The reasons behind this are currently under investigation by Herres-Pawlis et al.^[53]

Peroxo complex formation and characterisation

The copper(I) precursor was generated in situ from the starting compounds by following the synthetic route described by Herres-Pawlis et al.^[31] It should be noted that the direct synthesis of a Cu^I complex from $[Cu(MeCN)_4]SbF_6$ is possible, but this species does not activate dioxygen, since acetonitrile blocks the coordination site.^[11] The precursor $[Cu\{HC(3-tBuPz)_2(1-Melm)\}][SbF_6]$ was then injected into an O₂-saturated solution in dichloromethane at 195 K (Scheme 2). The formation of the resulting peroxide complex $[Cu_2O_2\{HC(3-tBuPz)_2(1-Melm)\}_2][SbF_6]_2$ ($P(SbF_6)_2$) was monitored by UV/Vis spectroscopy (Figure 3).

The spectrum shows absorption bands at $\lambda = 334$ and 534 nm. Time-dependent (TD) DFT calculations predict the positions of these bands perfectly. Moreover, the deep violet colour of the solution and the existence of UV/Vis bands in

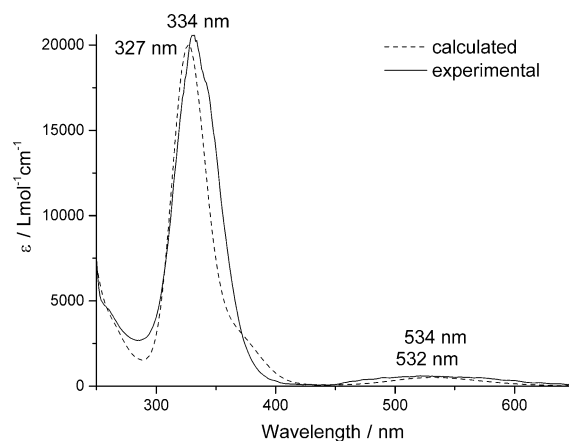


Figure 3. UV/Vis spectrum of the formation of $P(SbF_6)_2$ at 195 K (DFT: BS-TPSSH/6-31g(d)).

this region, separated by 200 nm, clearly show the formation of a peroxide complex. It is known from other copper(II) peroxide complexes that their UV/Vis spectra exhibit intense oxygen to copper charge-transfer (LMCT) absorptions, which are consistent with the presence of highly covalent Cu–O bonds.^[7] The real metalloproteins oxytyrosinase and oxyhemocyanin also show similar UV/Vis transitions.^[54,55] A striking difference, however, is the blueshift of the UV/Vis bands in comparison to those at $\lambda = 350$ and 550 nm for other known bis(pyrazolyl)methane peroxo complexes.^[27,31] To understand this phenomenon, NTO calculations were performed; the results are analysed below.^[56]

The species $P(SbF_6)_2$ could be generated in > 95 % yield at 195 K and was stable at that temperature for several days. Its half-life at 273 K is 3.5 min. Further analyses included cryo-ultrahigh resolution (cryo-UHR) ESI mass spectrometry (Figure 4), which also confirmed the formation of a $(\mu-\eta^2:\eta^2)$ -copper(II) peroxide core. The peroxo complex appears here as the monocationic species $P(SbF_6)^+$.

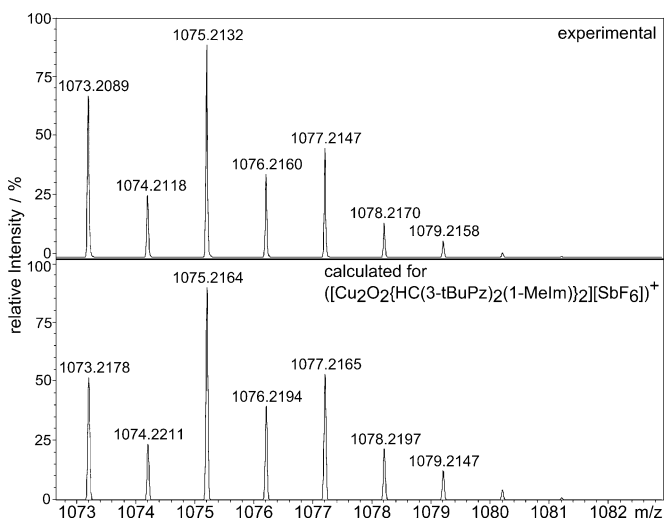


Figure 4. Cryo-UHR-ESI mass spectrum of $P(SbF_6)_2$ at 193 K.

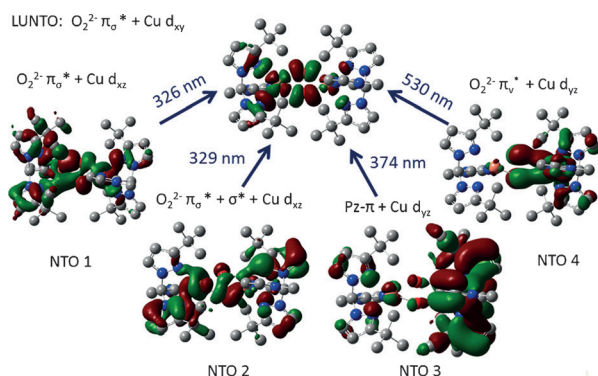


Figure 5. NTO analysis of **P** (Gaussian 09, BS-TPSSH/6-31g(d)). LUNTO = lowest unoccupied natural transition orbital

NTO calculations on the geometry-optimised coordinates were performed by using the TPSSH functional with broken symmetry combined with the 6-31g(d) basis set. Figure 5 shows the results of this calculation. LUNTO symbolises the orbital that accepts electrons in the transition process under investigation. NTO analysis was performed for the four major electronic transitions.

Those at $\lambda = 326$, 329 and 374 nm correspond to the transition at $\lambda = 334$ nm in the experimental spectrum, which is very accurate (see the Supporting Information for details). The second transition is also predicted very well because deviation from the experimental value is only 4 nm. Each NTO consists of fractions of several orbital types of copper and the oxygen peroxide unit. The LUNTO, for example, is composed of π_{σ}^* orbital parts at the oxygen atoms and d_{xy} orbitals at the copper atoms. The less intensive transition at $\lambda = 534$ nm originates from a NTO that shows oxygen π_{ν}^* and Cu d_{xy} characteristics (NTO 4). For NTO 1–3, it is not as easy to see the components that contribute to the transition orbital. The NTO 1 shows elements of π_{σ}^* at the oxygen atoms and those of d_{xz} at copper. In NTO 2, the same applies, with an additional peroxide- σ^* fraction. The NTO 3 does not incorporate any peroxide-orbital parts, but shows participation of the π system of the ligand. The TD-DFT calculations already predict blueshifted LMCT transitions. These can be explained by the strong donor ability of the imidazolyl moiety at the ligand. As Stack et al. reported in 2014, increased donation of the ligand to copper leads to an increase of the LUMO orbital energy, and therefore, results in a higher energetic transition, which appears blueshifted.^[57]

As a further characterisation method, we performed X-ray absorption experiments (XAS) at the copper K-edge.

Figure 6 shows the Cu K-edge X-ray absorption near-edge structure (XANES) spectrum of $\text{P}(\text{SbF}_6)_2$. Only a low-intensity pre-edge signal at 8978 eV is found in the spectrum. This excludes an oxidation state of Cu^{I} because the intensity is typical for a dipole-forbidden $1s \rightarrow 3d$ quadrupole transition characteristic of Cu^{II} .^[58–60] The $1s \rightarrow 4p + \text{LMCT}$ shake-down transition at 8987 eV^[61] is only present as a weak shoulder. It should be noted that Cu^{III} in related compounds is characterised by a sharp signal around this energy value,^[61] and a higher pre-peak intensity due to more available empty d states.^[62]

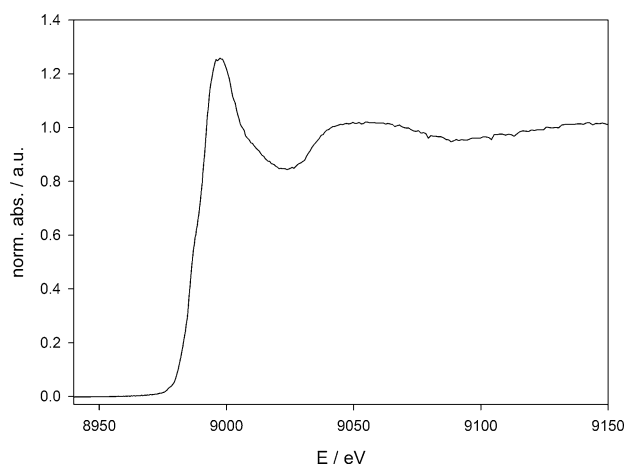


Figure 6. Copper K-edge XANES spectrum of $\text{P}(\text{SbF}_6)_2$.

Consequently, Cu^{III} can also be excluded and a Cu^{II} state is unequivocally concluded. The white-line morphology was similarly found by Solomon et al.^[63] and Meyer et al.^[64] for dinuclear $(\mu\text{-}\eta^2\text{-}\eta^2)$ side-on complexes.

The extended X-ray absorption fine structure (EXAFS) spectrum and corresponding Fourier-transformed function of $\text{P}(\text{SbF}_6)_2$ are given in Figure 7, and the extracted structural parameters are given in Table 3. The first contribution at an aver-

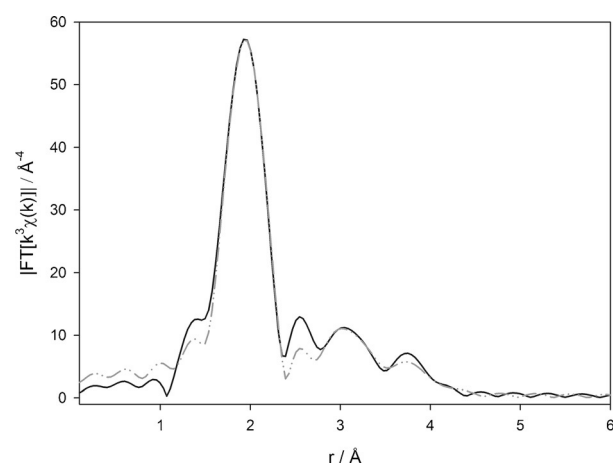


Figure 7. Fourier-transformed Cu K-edge EXAFS spectrum (black solid line: experimental data; grey dashed line: fitted function) of $\text{P}(\text{SbF}_6)_2$.

Table 3. Structural parameters obtained by fitting the experimental EXAFS functions with theoretical models.

	Abs-Bs ^[a]	N(Bs) ^[b]	$r(\text{Abs-Bs})$ ^[c] [Å]	σ^{d} [Å]	R^{e} [%]
$\text{P}(\text{SbF}_6)_2$	Cu-N/O	5.4 ± 0.5	1.99 ± 0.02	0.063 ± 0.006	15.05
	Cu-C/N	1.4 ± 0.2	2.92 ± 0.03	0.032 ± 0.003	
	Cu-C/N	4.6 ± 0.9	3.37 ± 0.03	0.112 ± 0.012	
	Cu-Cu	1.3 ± 0.4	3.69 ± 0.06	0.110 ± 0.033	

[a] Abs = X-ray absorbing atom. Bs = backscattering atom (neighbour).
 [b] Number of neighbour atoms. [c] Distance between Abs and Bs.
 [d] Debye–Waller-like factor to account for disorder. [e] Quality of fit.

age distance of 1.99 Å is composed of the two oxygen atoms from the side-on peroxy group and nitrogen atoms from the ligands. The next two shells at 2.92 and 3.37 Å are also combined C/N shells from the ligand and are in reasonable agreement with the DFT model. However, it should be noted that carbon and nitrogen at distances of around 3 Å are subjected to a rather large error in coordination numbers due to the low back-scattering amplitude.^[65] A Cu–Cu contribution at 3.69 Å with one back-scatterer within the error bar could be detected, which additionally proved the dimeric character of the complex in solution. This value is 0.12 Å larger than that in the DFT model of **P**. Considering the high noise level of the unfiltered spectra, which is caused by the low concentration of the copper species and the dichloromethane solvent, the agreement is quite good. Higher distance multiple scattering shells were removed by Fourier filtering.^[60,63]

Stoichiometric and catalytic hydroxylation

Functional enzymatic models not only need to incorporate a model of the active centre of the enzyme, but also be able to execute the catalytic reactions of those enzymes. As mentioned above, the catalytic reactivity of tyrosinase models is rare. We performed experiments to show both efficient stoichiometric oxidation of phenolates to catecholates at 193 K and catalytic oxidation of phenols to quinones at room temperature with triethylamine, through a reaction pathway consistent with the generally accepted enzymatic mechanism.^[5,31]

Following a standard protocol,^[24,30,66] the combination of 25 equivalents of 8-hydroxyquinoline and 50 equivalents of triethylamine under an oxygen pressure of 1 atm leads to the formation of 14 equivalents of the quinone in 20 min (Figure 8). With prolonged reaction time, the yield of the quinone decreases, presumably due to consecutive reactions of the highly reactive quinones, leading to a yield of 9 equivalents after 1 h and 7 equivalents after 16 and 18 h. The formation of the quinone was followed by UV/Vis spectroscopy, due to the strong UV/Vis band at $\lambda = 413$ nm ($\epsilon = 1000$ L mol⁻¹ cm⁻¹).^[67] This reaction proceeds on a millimolar scale and converts 80% of the added hydroxyquinoline into the quinone, which makes it synthetically useful. The addition of triethylamine or 8-hydroxyquinoline separately does not affect the lifetime of the **P** species. Only in combination does the hydroxylation reaction occur. Moreover, the formation of the **P** species can be observed when either triethylamine or 8-hydroxyquinoline is present. When both components are present, the **P** species does not appear, but the same catalytic hydroxylation reaction is observable by its strong quinone absorption as those observed when the components are added after **P** formation. This type of self-assembly has been observed previously for related **P** species.^[19,68] We also studied the potential influence of silver ions, but retrieving all AgCl by means of a syringe filter (0.45 μ m) did not change the results.

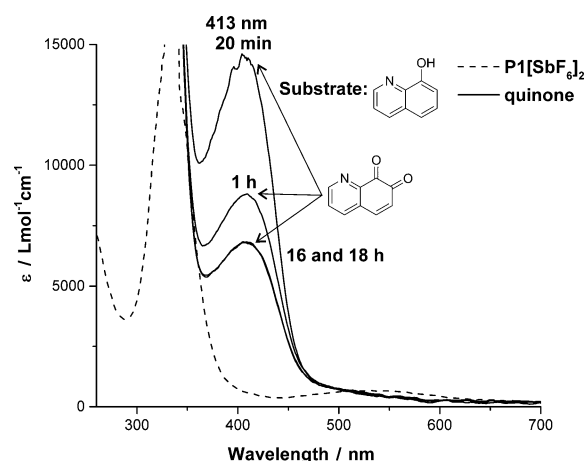


Figure 8. UV/Vis spectra of P(SbF₆)₂ (dashed) and of the formation of the quinone (black).

To investigate the kinetics of the hydroxylation step, we studied the stoichiometric hydroxylation reaction of **P** with various sodium phenolates. Excess oxygen was removed by N₂ purging before the substrate was added. All five substrates are quantitatively converted into the corresponding catechol within 20 min (see the Supporting Information). We detected a strong dependence of the reaction speed on the amount of substrate added. This typical substrate binding kinetics, depicted in Figure 9, has also been observed for the parent peroxy species.^[31] We assume that a phenolate–peroxy species forms as an intermediate.^[31] The related bis(μ -oxo) species was found to be energetically less favourable.^[52] Measuring the hydroxylation velocity at different substrate concentrations enables us to resolve the intrinsic hydroxylation constant, k_{ox} and the binding constant, K_{eq} .

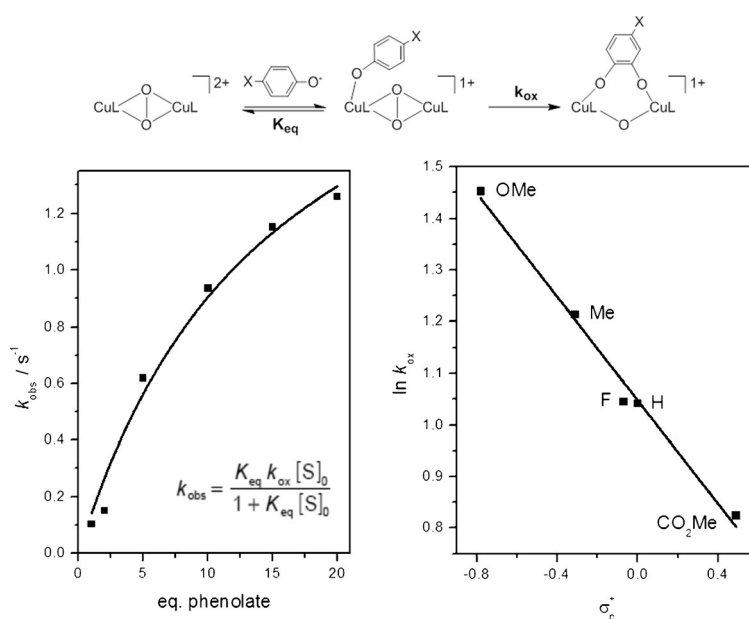


Figure 9. Top: Scheme of the substrate-binding kinetics. Left: Substrate binding and hydroxylation of *p*-carbomethoxyphenolate by P(SbF₆)₂; right: Hammett plot for the stoichiometric hydroxylation reaction with various *p*-substituted phenolates at 195 K.

Table 4. Hydroxylation constant, k_{ox} [s^{-1}], of both **P** species with *p*-X-phenolates.

X	ImPz-P	PyPz-P ^[31]
OMe	4.27	1.33
Me	3.36	0.87
F	2.84	0.73
H	2.83	0.65
CO ₂ Me	2.28	0.36

Table 4 provides a summary of the data for k_{ox} for the present **P** species and the parent species PyPz-P. It is remarkable that the intrinsic hydroxylation constant, k_{ox} of **P** for carbomethoxyphenolate could be determined as 2.28 s^{-1} (pyridinyl-peroxo: 0.36 s^{-1}) and the equilibrium constant, K_{eq} as 0.066 L mol^{-1} (pyridinyl-peroxo: 1.00 L mol^{-1}). For the same substrate, Itoh et al. reported a hydroxylation constant of 0.083 s^{-1} with a **P** species stabilised by a tridentate bis(pyridinyl)benzylamine ligand, L^{Py2bz}.^[23] For fluorophenolate, they reported a value of 0.63 s^{-1} . For a $\mu\text{-}\eta^1\text{:}\eta^1\text{-peroxo}$ species, stoichiometric hydroxylation reactivity was reported with hydroxylation constants that were at least one magnitude smaller.^[25] With regard to real tyrosinase, Garcia-Canovas et al. reported k_{cat} values for 25°C in a buffer solution that were five times larger.^[69] Taking into account that the biological reaction proceeds at a temperature 100 K higher than that of biomimetic systems, it is clear that the new system comes very close to the biological reaction speed.

Furthermore, a correlation of the obtained k_{ox} values against the corresponding Hammett parameters (Figure 9) gave a reaction constant, ρ , of -0.5 , which proved that the reaction proceeded electrophilically, as mediated by tyrosinase with a ρ value of -1.75 .^[69] The parent peroxo species possesses a ρ of -1 .^[31]

Moreover, it shows the superior hydroxylation reactivity of **P** in comparison to the pyridinyl-peroxo species, which is directly related to exchange of the third donor function pyridinyl against the imidazolyl moiety. The stronger donor ability enhances the oxidative force of **P**, which leads to faster hydroxylation in the catalytic mode, but also to the observed subsequent reactions.

Conclusion

We have reported that fine-tuning of biomimetic ligands leads to enhanced catalytic activity of a catalytic tyrosinase model. We have provided syntheses and structural characterisation of a new bis(pyrazolyl)imidazolylmethane ligand and its copper(II) halide complexes. The reaction of dioxygen with its copper(I) hexafluoroantimonate complex gives a peroxo species that has been characterised by UV/Vis and XAS spectroscopy as well as cryo-UHR-ESI mass spectrometry. The classical CT absorptions are strongly blueshifted and have been analysed by TD-DFT and NTO analysis. They show the special role of the third donor function. The new peroxo species displays stoichiometric and catalytic hydroxylation activity. The catalytic activity towards 8-hydroxyquinoline is more rapid than that observed

for the parent pyridinyl-peroxo species. Analysis of the substrate-binding kinetics quantitatively proves that the electron-deficient substrate *p*-carbomethoxyphenolate is hydroxylated approximately six times faster. This possibility of efficiently tuning catalytic activity by donor exchange opens up new directions for industrial applications of this mild, selective and atom-economic hydroxylation chemistry.

Experimental Section

General

All experiments involving moisture- and air-sensitive compounds were carried out by using standard Schlenk techniques. All chemicals were purchased from Sigma-Aldrich, Alfa-Aesar, Acros Organics, Applichem, Fluka or ABCR and were used as received without further purification. The solvents used were dried by standard literature procedures.^[70] The starting materials 3-*tert*-butylpyrazole,^[71] 1-methyl-2-imidazolecarboxaldehyde^[72] and CuCl^[73] were synthesised according to procedures reported in the literature. For the catalytic conversion of phenolates, the substituted phenols were deprotonated with a solution of NaOH, according to a procedure reported in the literature.^[74]

Physical methods

Cryospray-ionisation MS (CSI-MS) measurements were performed on a UHR-TOF Bruker Daltonik (Bremen, Germany) maXis plus 5G instrument, which was an ESI-TOF mass spectrometer capable of a resolution of at least 60000 full-width at half-maximum (FWHM), coupled to a Bruker Daltonik Cryospray unit. Detection was in positive-ion mode and the source voltage was 4.5 kV. The flow rates were $250 \mu\text{L h}^{-1}$. The drying gas (N_2), to aid solvent removal, was held at 198 K and the spray gas was held at 193 K. The machine was calibrated prior to every experiment through direct infusion of the Agilent ESI-TOF low concentration tuning mixture, which provided an m/z range of singly charged peaks up to 2700 Da in both ion modes. Fast-atom bombardment (FAB) mass spectra were obtained with a Thermo Finnigan MAT 95 or a Jeol MStation sector field mass spectrometer. Ionisation was achieved with accelerated xenon atoms (8 kV) in a glycerin or 2-nitrobenzylalcohol matrix on a copper target. For low-resolution measurements, the resolution was about 1000 and for high resolution at about 5000. Depending on the method, areas between 40 and 3040 u were recorded. ESI mass spectra were obtained on a Thermo Finnigan LTQ Ultra Fourier-transform ion cyclotron resonance mass spectrometer. Resolution was adjusted to 100000 at m/z 400. Depending on the method, areas between 50 and 2000 u were recorded. ESI measurements were performed at an IonMax ionic source with an ESI head. The source voltage was 4 kV with a spray capillary temperature of 523 K, a sheath-gas flow rate of 25 and a sweep-gas flow rate of 5 units. IR spectra were recorded with a Jasco FTIR 460 spectrophotometer in the range of $650\text{--}3500 \text{ cm}^{-1}$. Measurements took place at room temperature in the ATR measurement mode. UV/Vis spectra were recorded with a Varian Cary 60 spectrophotometer from Agilent Technologies in combination with a fibre-optic quartz glass immersion probe (Hellma, 1 mm) in a customised Schlenk measurement cell. Elemental analyses were performed with a Vario EL or Vario MICRO CHNS analyser.

X-ray absorption measurements

Measurements at the Cu K-edge were carried out at beamline BM23 of the European Synchrotron Radiation Facility ESRF (Grenoble, France) in fluorescence mode by making use of a hyperpure solid-state Ge detector. The sample was measured as a frozen solution at liquid nitrogen temperature by using CH₂Cl₂ as a matrix. Due to the low concentration of 0.01 mol L⁻¹, several scans were conducted and averaged to increase the signal to noise ratio. Data reduction followed standard procedures given in ref. [59]. Due to the high residual noise, Fourier filtering was applied in the range $\Delta r = 3\text{--}11.5 \text{ \AA}$.

X-ray diffraction analyses

The crystal data for **L**, **C1** and **C2** are presented in Table 5. The data for **L** and **C2** were collected with an Oxford KM4 XCalibur2 diffractometer and for **C1** with a Bruker D8 Venture diffractometer with graphite monochromated Mo_{K α} radiation ($\lambda = 0.71073 \text{ \AA}$). Data reduction and absorption correction was performed with the programs CRYCALIS (Oxford, 2008) and CRYCALIS RED (Oxford, 2008; **L** and **C2**) or with SAINT and SADABS (**C1**).^[75] The structure was solved by direct and conventional Fourier methods and all non-hydrogen atoms were refined anisotropically with full-matrix least-squares based on F^2 (XPREP,^[76] SHELXS^[77] and ShelXle^[78]). Hydrogen atoms were derived from difference Fourier maps and placed at idealised positions, riding on their parent C atoms, with isotropic displacement parameters of $U_{\text{iso}}(\text{H}) = 1.2 U_{\text{eq}}(\text{C})$ and $1.5 U_{\text{eq}}(\text{C methyl})$. All methyl groups were allowed to rotate, but not tip.

Table 5. Crystallographic data and parameters of **L**, **C1** and **C2**.

	L	C1	C2
formula	C ₁₉ H ₂₈ N ₆	C ₁₉ H ₂₈ Cl ₂ CuN ₆	C ₂₁ H ₃₁ Br ₂ CuN ₇
M_r [g mol ⁻¹]	340.47	474.91	604.89
crystal size [mm]	0.37 × 0.31 × 0.10	0.0 × 0.04 × 0.04	0.26 × 0.24 × 0.19
T [K]	173(2)	173(2)	173(2)
crystal system	triclinic	triclinic	monoclinic
space group	$P\bar{1}$	$P\bar{1}$	Cc
a [Å]	6.3373(4)	7.6934(6)	12.5876(4)
b [Å]	10.2663(4)	8.0918(7)	14.4039(6)
c [Å]	14.8859(7)	18.1881(15)	14.6325(5)
α [°]	84.201(4)	89.787(2)	90
β [°]	87.172(4)	88.0722(2)	103.298(4)
γ [°]	88.343(3)	84.734(2)	90
V [Å ³]	961.53(7)	1126.85(16)	2581.89(16)
Z	2	2	4
ρ_{calcd} [g cm ⁻³]	1.176	1.400	1.556
μ [mm ⁻¹]	0.074	1.223	3.963
λ [Å]	0.71073	0.71073	0.71073
$F(000)$	368	494	1220
hkl range	-6/7, -12/10, ±18	±9, ±10, ±22	-15/14, -16/17, -17/16
reflns collected	5216	20053	6403
independent reflns	3882	4623	3583
R_{int}	0.0149	0.0511	0.0286
reflns observed	3882	4623	3583
no. parameters	233	260	288
R_1 [$I \geq 2\sigma(I)$]	0.0499	0.0460	0.0295
wR_2 (all data)	0.1350	0.1128	0.0648
goodness-of-fit	1.037	1.085	1.068
largest diff. peak, hole [e Å ⁻³]	-0.213, 0.229	-0.512, 0.882	-0.431, 0.405

CCDC-1057372 **L**, 1057370 **C1** and 1057371 **C2** contain the supplementary crystallographic data for this paper. These data are provided free of charge by The Cambridge Crystallographic Data Centre.

Computational details

DFT calculations were performed with the program suite Gaussian 09.^[49] The geometries of **L**, **C1**, **C2** and the peroxo species were optimised (Table 1) by using the nonlocal hybrid meta GGA TPSSH functional^[79] and the double-zeta basis set 6-31g(d), as implemented in Gaussian 09 on all atoms. The starting geometries for **L** and complexes **C1** and **C2** were generated from the molecular structures. The **P** conformer geometries were derived from those of the parent pyrazolyl-pyridinyl **P** species. Energetic evaluation of the **P** conformers was also done with TPSSH/def2-TZVP. Frequency calculations did not show imaginary values. NBO calculations for the complexes were accomplished by using the program suite NBO 6.0.^[50,51,80] Continuous spectra were plotted with the AOMix program.^[81,82] The intensities were normalised to the experimental spectrum. For the **P** species, we searched for energetically low-lying unrestricted Kohn–Sham (UKS) wavefunctions with broken spin and spatial symmetry (“broken-symmetry” wavefunctions) by using the “guess = mix” keyword.

HC(3-*t*BuPz)₂(1-Melm) (**L**)

3-*tert*-Butylpyrazole (5.00 g, 0.40 mol, 2 equiv) was added in small portions to a slurry of NaH (1.00 g, 0.42 mol, 2.1 equiv) in freshly distilled, dry THF (50 mL) at 273 K under vigorous stirring, until no more gas evolution was visible. Next, thionylchloride (1.50 mL, 0.20 mol, 1 equiv) was added dropwise to the yellow suspension at 273 K and stirred first at 273 K for 30 min and afterwards at room temperature for another 45 min. 1-Methylimidazole-2-carboxaldehyde (2.20 g, 0.20 mol, 1 equiv) and catalytic amounts of CoCl₂ were added before the mixture was heated at reflux overnight and the evolution of SO₂ gas was visible. The solution changed colour to red–orange. After cooling the reaction mixture to room temperature, water (50 mL) and diethyl ether (50 mL) were added, followed by 2 h of stirring. Lastly, the combined organic phases were extracted with diethyl ether (3 × 45 mL) and washed with water (2 × 50 mL) and brine (2 × 50 mL). The combined organic phases were dried over Na₂SO₄ and the solvent was reduced in vacuo. The product was obtained by vacuum distillation (313 K, 1.4×10^{-2} bar) in the second fraction in good yield (4.7 g, 0.14 mol, 70%). Single crystals obtained from the mixture were characterised by XRD analysis. ¹H NMR (400 MHz, CDCl₃, 298 K): $\delta = 1.26$ (s, 18H; 3-*t*BuPz), 3.45 (s, 3H; Melm), 6.15 (d, ³J(H,H) = 2.5 Hz, 2H; 4H-*t*BuPz), 6.87 (d, ³J(H,H) = 1.2 Hz, 1H; 5H-Melm), 7.04 (d, ³J(H,H) = 1.2 Hz, 1H; 4H-Melm), 7.44 (d, ³J(H,H) = 2.5 Hz, 2H; 5H-*t*BuPz), 7.64 ppm (s, 1H; CH); ¹³C NMR (100 MHz, CDCl₃, 298 K): $\delta = 30.6$ (CH₃-*t*BuPz), 32.2 (C-*t*BuPz), 33.1 (CH₃-Melm), 71.5 (CH(ap.)), 103.5 (4C-*t*BuPz), 122.8 (5C-Melm), 128.0 (4C-Melm), 129.4 (5C-*t*BuPz), 142.0 (2C-Melm), 163.1 ppm (3C-*t*BuPz); IR (ATR): $\tilde{\nu} = 2959$ (w, CH_{arom}), 2928 (w, CH_{arom}), 2902 (w, CH_{arom}), 2866 (vw, CH_{aliph}), 1531 (w), 1519 (m), 1501 (w), 1478 (w), 1461 (w), 1400 (w), 1362 (w), 1335 (m), 1317 (w), 1281 (w), 1244 (m), 1225 (w), 1206 (w), 1189 (w), 1153 (m), 1135 (w), 1046 (m), 1022 (w), 993 (w), 927 (w), 852 (w), 818 (m), 805 (s), 762 (vs), 724 (m), 698 (m), 664 cm⁻¹ (w); MS (ESI⁺, acetone): m/z (%): 364 (17) [$M + H + Na$]⁺, 363 (100) [$M + Na$]⁺, 341 (42) [$M + H$]⁺, 218 (10) [$C_{10}H_{19}N_4 + Na$]⁺, 217 (96) [$C_{12}H_{17}N_4$]⁺, 214 (1) [$C_{13}H_{16}N_3$]⁺; HRMS (ESI⁺, acetone): m/z calcd for C₁₉H₂₈N₆Na [$M + Na$]⁺: 363.2273; found: 363.2273; elemental analysis calcd (%) for C₁₉H₂₈N₆ (340.48 g mol⁻¹): C 67.0, H 8.3, N 24.7; found: C 67.1, H 8.3, N 24.3.

[CuCl₂{HC(3-*t*BuPz)₂(1-Melm)}] (C1)

Copper(II) chloride (0.17 g, 1.00 mmol) was suspended in methanol (5 mL), resulting in a green–brown slurry. A solution of **L** (0.34 g, 1.00 mmol) dissolved in methanol (5 mL) was added dropwise to the copper-salt mixture and after stirring for 16 h at room temperature a deep-green solid precipitated. Storage of the mixture at room temperature resulted in single crystals suitable for XRD analysis (0.14 g, 0.29 mmol, 30%). IR (ATR): $\tilde{\nu}$ = 3100 (vw, CH_{arom}), 2902 (w, CH_{arom}), 2865 (w, CH_{aliph}), 1518 (m), 1474 (w), 1459 (w), 1417 (w), 1350 (m), 1229 (m), 1204 (w), 1152 (w), 1081 (w), 1054 (w), 970 (w), 861 (m), 831 (w), 811 (m), 803 (vs), 782 (vs), 770 (vs), 756 (m), 728 (w), 699 (m), 669 (w), 634 (w), 627 (w), 614 (m), 603 cm⁻¹ (m); MS (FAB⁺): *m/z* (%): 440 (16) [⁶³Cu³⁷CIL]⁺ and [⁶⁵Cu³⁵CIL]⁺, 438 (20) [⁶³Cu³⁵CIL]⁺, 405 (20) [⁶⁵CuL]⁺, 403 (40) [⁶³CuL]⁺, 342 (15) [L]⁺, 217 (100) [HC(3-*t*BuPz)(1-Melm)]⁺; elemental analysis calcd (%) for C₁₉H₂₈Cl₂CuN₆ (474.92 g mol⁻¹): C 48.1, H 5.9, N 17.7; found: C 47.9, H 6.0, N 17.7.

[CuBr₂{HC(3-*t*BuPz)₂(1-Melm)}]·MeCN (C2)

An orange solution of **L** (0.17 g, 0.50 mmol) dissolved in THF (1 mL) was added dropwise to a deep-green solution of copper(II) bromide (0.11 g, 0.50 mmol) dissolved in acetonitrile (2 mL). The solution was stirred at room temperature for 3 h, which resulted in the precipitation of a brown solid. The solid was recrystallised from acetonitrile (4 mL) by making sure to cool the solution slowly (over 5 h). Storage of the solution at 241 K resulted in small brown crystals suitable for XRD analysis after 4 d (0.21 g, 0.35 mmol, 70%). IR (ATR): $\tilde{\nu}$ = 3118 (w, CH_{arom}), 3101 (w, CH_{arom}), 2966 (m, CH_{arom}), 2908 (w, CH_{arom}), 2867 (w, CH_{aliph}), 1737 (vw), 1639 (w), 1552 (w), 1523 (m), 1516 (m), 1484 (m), 1459 (m), 1415 (m), 1362 (m), 1345 (m), 1335 (w), 1286 (w), 1232 (vs), 1207 (m), 1156 (m), 1084 (m), 1067 (m), 1030 (w), 1018 (w), 986 (w), 971 (m), 928 (vw), 861 (m), 833 (m), 804 (vs), 774 (vs), 725 (m), 699 (s), 669 cm⁻¹ (w); MS (FAB⁺): *m/z* (%): 744 (11) [C₃₈H₅₆N₁₂⁶³Cu]⁺, 487 (3) [C₁₈¹³CH₂₈N₆⁶⁵Cu⁸¹Br]⁺, 486 (12) [C₁₉H₂₈N₆⁶⁵Cu⁸¹Br]⁺, 485 (10) [C₁₈¹³CH₂₈N₆⁶³Cu⁸¹Br]⁺, [C₁₈¹³CH₂₈N₆⁶⁵Cu⁷⁹Br]⁺, 484 (37) [C₁₉H₂₈N₆⁶³Cu⁸¹Br]⁺, [C₁₉H₂₈N₆⁶⁵Cu⁷⁹Br]⁺, 483 (8) [C₁₈¹³CH₂₈N₆⁶³Cu⁷⁹Br]⁺, 482 (26) [C₁₉H₂₈N₆⁶³Cu⁷⁹Br]⁺, 403 (76) [C₁₉H₂₈N₆⁶³Cu]⁺, 341 (100) [C₁₉H₂₉N₆]⁺, 217 (100) [C₁₂H₁₇N₄]⁺; elemental analysis calcd (%) for C₁₉H₂₈N₆CuBr₂ (563.83 g mol⁻¹): C 40.47, H 5.01, N 14.91; found: C 40.52, H 5.17, N 14.28.

[Cu₂O₂{HC(3-*t*BuPz)₂(1-Melm)}₂][SbF₆]₂ (P(SbF₆)₂)

A solution of **L** (0.16 mmol, 54 mg) dissolved in CH₂Cl₂ (5 mL) was added in one portion to CuCl (0.17 mmol, 17 mg). The resulting suspension was stirred for 45 min to 1 h. With vigorous shaking, a solution of AgSbF₆ (0.17 mmol, 61 mg) dissolved in THF (250 μL) was added and AgCl precipitated to produce the precursor solution. This solution could be filtered through a syringe filter (VWR, 130 mm, 0.45 μm). CH₂Cl₂ (10 mL) was added to a UV/Vis measurement cell and cooled to 195 K. Oxygen was bubbled through the solvent for 5 min to generate an oxygen-saturated solution before the precursor solution (1 mL) was added, resulting in an immediate colour change to deep violet. Formation of the peroxide complex was followed by UV/Vis spectroscopy.

Catalytic reaction of P(SbF₆)₂ with 8-hydroxyquinoline

Compound P(SbF₆)₂ was prepared as described above and its development was followed by UV/Vis spectroscopy. After stabilisation of the optical spectrum, a solution containing 8-hydroxyquinoline

(25 equiv) and NEt₃ (50 equiv) in CH₂Cl₂ (200 μL) was added. The reaction solution was warmed to room temperature, stirred overnight and monitored by means of UV/Vis spectroscopy throughout; an intense feature at λ = 413 nm owing to the formation of the corresponding quinone was observed.^[67] After 16–18 h, the reaction was quenched with 0.5 M HCl (3 mL). The aqueous solution was extracted with CH₂Cl₂ (3 × 3 mL) and the combined organic phases were dried over MgSO₄. The solvent was reduced in vacuo, followed by NMR spectroscopic characterisation.^[31] The quantity of the quinone formed was determined from the extinction coefficient of the quinone, yielding 14 turnovers per dinuclear copper peroxide species after 20 min. The 7,8-dione of quinoline was detected by HRMS (EI): *m/z* calcd for C₉H₅O₂N: 159.0319; found: 159.0310, which corresponded to the quinone with the appropriate calculated isotope. ¹H NMR (400 MHz, CD₃OD): δ = 6.90 (m, 1 H), 7.80 (m, 1 H), 7.92 (m, 1 H), 8.20 (m, 1 H), 8.54 ppm (m, 1 H).

Stoichiometric reaction of P(SbF₆)₂

The reactions of P(SbF₆)₂ with sodium *p*-X-phenolates (X = H, CO₂Me, OMe, Me, F) at 195 K ([P(SbF₆)₂] = 1 mM, [substrate] = 1, 2, 5, 10, 15 and 20 equiv per dimer) were optically monitored by following the decay of the peroxide species until no change in the absorption spectrum was evident. In all reactions, solutions of P(SbF₆)₂ were prepared by the “injection” method at 195 K to give a final volume of 10 mL. After stabilisation of the optical spectrum, excess O₂ was removed by five cycles of vacuum/N₂ purging and five min of purging the solution with N₂. The substrate solutions were added quickly in one portion. The data for each reaction were reasonably fitted with a single exponential to obtain the pseudo-first-order rate constant, *k*_{obs}. The saturation behaviour of *k*_{obs} with respect to [phenolate] was fitted to the equation in Figure 9 to obtain the rate constant for the oxidation reaction, *k*_{ox} and the association constant, *K*_{eq}. Substrate characterisation was performed as described previously.^[31] The resulting NMR spectra are given in the Supporting Information.

Acknowledgements

Financial support by the Deutsche Forschungsgemeinschaft (DFG) (DFG-FOR1405 and SFB749-B10) is gratefully acknowledged. Calculation time is gratefully acknowledged from the OCuLUS Cluster at the PC² Paderborn and the Leibniz-Rechenzentrum München. M.B. gratefully acknowledges provision of beamtime by the European Radiation Synchrotron Facility (ESRF, Grenoble, France), and we also thank Olivier Maton and Dr. Suresh Gatla for help during the measurements. I.I.-B. and M.D. gratefully acknowledge support through the “Solar Technologies Go Hybrid” initiative of the State of Bavaria. S.H.-P. and C.W. thank Ulrich Herber for help with NMR spectroscopy measurements.

Keywords: copper · biomimetic synthesis · kinetics · N ligands · structure–activity relationships

- [1] L. Que, Jr., W. B. Tolman, *Nature* **2008**, *455*, 333–340.
- [2] B. Wu, *Curr. Top. Med. Chem.* **2014**, *14*, 1425–1449.
- [3] Y. Matoba, T. Kumagai, A. Yamamoto, H. Yoshitsu, M. Sugiyama, *J. Biol. Chem.* **2006**, *281*, 8981–8990.
- [4] M. Rolff, J. Schottenheim, H. Decker, F. Tuzcek, *Chem. Soc. Rev.* **2011**, *40*, 4077–4098.

- [5] R. H. Holm, P. Kennepohl, E. I. Solomon, *Chem. Rev.* **1996**, *96*, 2239–2314.
- [6] E. I. Solomon, D. E. Heppner, E. M. Johnston, J. W. Ginsbach, J. Cirera, M. Qayyum, M. T. Kieber-Emmons, C. H. Kjaergaard, R. G. Hadt, L. Tian, *Chem. Rev.* **2014**, *114*, 3659–3853.
- [7] L. M. Mirica, X. Ottenwaelder, T. D. P. Stack, *Chem. Rev.* **2004**, *104*, 1013–1045.
- [8] H.-C. Liang, M. J. Henson, L. Q. Hatcher, M. A. Vance, C. X. Zhang, D. Lahti, S. Kaderli, R. D. Sommer, A. L. Rheingold, A. D. Zuberbühler, E. I. Solomon, K. D. Karlin, *Inorg. Chem.* **2004**, *43*, 4115–4117.
- [9] L. Q. Hatcher, M. A. Vance, A. A. Narducci Sarjeant, E. I. Solomon, K. D. Karlin, *Inorg. Chem.* **2006**, *45*, 3004–3013.
- [10] N. Kitajima, K. Fujisawa, Y. Moro-oka, K. Toriumi, *J. Am. Chem. Soc.* **1989**, *111*, 8975–8976.
- [11] K. Fujisawa, T. Ono, Y. Ishikawa, N. Amir, Y. Miyashita, K. Okamoto, N. Lehnert, *Inorg. Chem.* **2006**, *45*, 1698–1713.
- [12] T. D. P. Stack, *Dalton Trans.* **2003**, *34*, 1881–1889.
- [13] T. Osako, K. Ohkubo, M. Taki, Y. Tachi, S. Fukuzumi, S. Itoh, *J. Am. Chem. Soc.* **2003**, *125*, 11027–11033.
- [14] J. Becker, P. Gupta, F. Angersbach, F. Tuczek, C. Näther, M. C. Holthausen, S. Schindler, *Chem. Eur. J.* **2015**, *21*, 11735–11744.
- [15] D. J. E. Spencer, A. M. Reynolds, P. L. Holland, B. A. Jazdzewski, C. Duboc-Toia, L. Le Pape, S. Yokota, Y. Tachi, S. Itoh, W. B. Tolman, *Inorg. Chem.* **2002**, *41*, 6307–6321.
- [16] S. Herres-Pawlis, U. Flörke, G. Henkel, *Eur. J. Inorg. Chem.* **2005**, *2005*, 3815–3824.
- [17] S. Herres-Pawlis, S. Binder, A. Eich, R. Haase, B. Schulz, G. Wellenreuther, G. Henkel, M. Rübhausen, W. Meyer-Klaucke, *Chem. Eur. J.* **2009**, *15*, 8678–8682.
- [18] A. Hoffmann, S. Herres-Pawlis, *Z. Anorg. Allg. Chem.* **2013**, *639*, 1426–1432.
- [19] C. Wilfer, P. Liebhäuser, H. Erdmann, A. Hoffmann, S. Herres-Pawlis, *Eur. J. Inorg. Chem.* **2015**, 494–502.
- [20] A. Hoffmann, U. Flörke, S. Herres-Pawlis, *Eur. J. Inorg. Chem.* **2014**, 2296–2306.
- [21] L. Casella, M. Gullotti, R. Radaelli, P. Di Gennaro, *J. Chem. Soc. Chem. Commun.* **1991**, *22*, 1611–1612.
- [22] L. Santagostini, M. Gullotti, E. Monzani, L. Casella, R. Dillinger, F. Tuczek, *Chem. Eur. J.* **2000**, *6*, 519–522.
- [23] S. Itoh, H. Kumei, M. Taki, S. Nagatomo, T. Kitagawa, S. Fukuzumi, *J. Am. Chem. Soc.* **2001**, *123*, 6708–6709.
- [24] M. Réglie, C. Jorand, B. Waegell, *J. Chem. Soc. Chem. Commun.* **1990**, *24*, 1752–1755.
- [25] G. Battaini, M. De Carolis, E. Monzani, F. Tuczek, L. Casella, *Chem. Commun.* **2003**, 726–727.
- [26] G. Battaini, E. Monzani, L. Casella, E. Lonardi, A. W. J. W. Tepper, G. W. Canters, L. Bubacco, *J. Biol. Chem.* **2002**, *277*, 44606–44612.
- [27] S. Palavicini, A. Granata, E. Monzani, L. Casella, *J. Am. Chem. Soc.* **2005**, *127*, 18031–18036.
- [28] A. Spada, S. Palavicini, E. Monzani, L. Bubacco, L. Casella, *Dalton Trans.* **2009**, 6468–6471.
- [29] I. Garcia-Bosch, A. Company, J. R. Frisch, M. Torrent-Sucarrat, M. Cardellach, I. Gamba, M. Güell, L. Casella, L. Que Jr, X. Ribas, J. M. Luis, M. Costas, *Angew. Chem. Int. Ed.* **2010**, *49*, 2406–2409; *Angew. Chem.* **2010**, *122*, 2456–2459.
- [30] M. Roff, J. Schottenheim, G. Peters, F. Tuczek, *Angew. Chem. Int. Ed.* **2010**, *49*, 6438–6442; *Angew. Chem.* **2010**, *122*, 6583–6587.
- [31] A. Hoffmann, C. Citek, S. Binder, A. Goos, M. Rübhausen, O. Troeppner, I. Ivanović-Burmazović, E. C. Wasinger, T. D. P. Stack, S. Herres-Pawlis, *Angew. Chem. Int. Ed.* **2013**, *52*, 5398–5401; *Angew. Chem.* **2013**, *125*, 5508–5512.
- [32] J. Schottenheim, N. Fateeva, W. Thimm, J. Krahmer, F. Tuczek, *Z. Anorg. Allg. Chem.* **2013**, *639*, 1491–1497.
- [33] J. N. Hamann, F. Tuczek, *Chem. Commun.* **2014**, *50*, 2298–2300.
- [34] J. N. Hamann, M. Roff, F. Tuczek, *Dalton Trans.* **2015**, *44*, 3251–3258.
- [35] K. V. N. Esguerra, Y. Fall, J.-P. Lumb, *Angew. Chem. Int. Ed.* **2014**, *53*, 5877–5881; *Angew. Chem.* **2014**, *126*, 5987–5991.
- [36] K. V. N. Esguerra, Y. Fall, L. Petitjean, J.-P. Lumb, *J. Am. Chem. Soc.* **2014**, *136*, 7662–7668.
- [37] B. Xu, J.-P. Lumb, B. A. Arndtsen, *Angew. Chem. Int. Ed.* **2015**, *54*, 4208–4211; *Angew. Chem.* **2015**, *127*, 4282–4285.
- [38] T. N. Sorrell, *Tetrahedron* **1989**, *45*, 3–68.
- [39] T. N. Sorrell, W. E. Allen, P. S. White, *Inorg. Chem.* **1995**, *34*, 952–960.
- [40] Y. Lee, G. Y. Park, H. R. Lucas, P. L. Vajda, K. Kamaraj, M. A. Vance, A. E. Milligan, J. S. Woertink, M. A. Siegler, A. A. Narducci Sarjeant, L. N. Zakharov, A. L. Rheingold, E. I. Solomon, K. D. Karlin, *Inorg. Chem.* **2009**, *48*, 11297–11309.
- [41] A. Arnold, C. Limberg, R. Metzinger, *Inorg. Chem.* **2012**, *51*, 12210–12217.
- [42] A. Arnold, R. Metzinger, C. Limberg, *Chem. Eur. J.* **2015**, *21*, 1198–1207.
- [43] C. Citek, C. T. Lyons, E. C. Wasinger, T. D. P. Stack, *Nat. Chem.* **2012**, *4*, 317–322.
- [44] A. Hoffmann, U. Flörke, M. Schürmann, S. Herres-Pawlis, *Eur. J. Org. Chem.* **2010**, 4136–4144.
- [45] L. Yang, D. R. Powell, R. P. Houser, *Dalton Trans.* **2007**, 955–964.
- [46] M. Wagner, C. Limberg, T. Tietz, *Chem. Eur. J.* **2009**, *15*, 5567–5576.
- [47] D. W. Randall, S. DeBeer George, B. Hedman, K. O. Hodgson, K. Fujisawa, E. I. Solomon, *J. Am. Chem. Soc.* **2000**, *122*, 11620–11631.
- [48] M. Kujime, C. Izumi, M. Tomura, M. Hada, H. Fujii, *J. Am. Chem. Soc.* **2008**, *130*, 6088–6098.
- [49] M. J. Frisch, G. W. Trucks, G. E. Schlegel, G. E. Scuseria, M. A. Robb, J. R. Cheeseman, G. Scalmani, V. Barone, B. Mennucci, G. A. Petersson, H. Nakatsuji, M. Caricato, X. Li, P. Hratchian, A. F. Izmaylov, J. Bloino, G. Zheng, J. L. Sonnenberg, M. Hada, M. Ehara, K. Toyota, R. Fukuda, J. Hasegawa, M. Ishida, T. Nakajima, Y. Honda, O. Kitao, H. Nakai, T. Vreven, J. A. J. Montgomery, J. E. Peralta, F. Ogliaro, M. Bearpark, J. J. Heyd, E. Brothers, K. N. Kudin, V. N. Staroverov, T. Keith, R. Kobayashi, J. Normand, K. Raghavachari, A. Rendell, J. C. Burant, S. S. Iyengar, J. Tomasi, M. Cossi, N. Rega, J. M. Millam, M. Klene, J. E. Knox, J. B. Cross, V. Bakken, C. Adamo, J. Jaramillo, R. Gomperts, R. E. Stratmann, O. Yazyev, A. J. Austin, R. Cammi, C. Pomelli, J. W. Ochterski, R. L. Martin, K. Morokuma, V. G. Zakrzewski, G. A. Voth, P. Salvador, J. J. Dannenberg, S. Dapprich, A. D. Daniels, O. Farkas, J. B. Foresman, J. V. Ortiz, J. Cioslowski, D. J. Fox, Gaussian 09, Revision D.01, Gaussian Inc., Wallingford CT, **2013**.
- [50] E. D. Glendening, J. K. Badenhop, A. E. Reed, J. E. Carpenter, J. A. Bohmann, C. M. Morales, C. R. Landis, F. Weinhold, *NBO 6.0*, Theoretical Chemistry Institute, University of Wisconsin: Madison, **2013**.
- [51] E. D. Glendening, C. R. Landis, F. Weinhold, *J. Comput. Chem.* **2013**, *34*, 1429–1437.
- [52] A. Hoffmann, S. Herres-Pawlis, *Chem. Commun.* **2014**, *50*, 403–405.
- [53] A. Hoffmann, C. Wilfer, S. Herres-Pawlis, unpublished results.
- [54] R. S. Himmelwright, N. C. Eickman, C. D. LuBien, K. Lerch, E. I. Solomon, *J. Am. Chem. Soc.* **1980**, *102*, 7339–7344.
- [55] K. Heirwegh, H. Borginon, R. Lontie, *Biochim. Biophys. Acta* **1961**, *48*, 506–517.
- [56] R. L. Martin, *J. Chem. Phys.* **2003**, *118*, 4775–4777.
- [57] C. Citek, B.-L. Lin, T. E. Phelps, E. C. Wasinger, T. D. P. Stack, *J. Am. Chem. Soc.* **2014**, *136*, 14405–14408.
- [58] K. C. C. Kharas, D.-J. Liu, H. J. Robota, *Catal. Today* **1995**, *26*, 129–145.
- [59] A. B. Ene, M. Bauer, T. Archipov, E. Roduner, *Phys. Chem. Chem. Phys.* **2010**, *12*, 6520–6531.
- [60] L.-S. Kau, D. J. Spira-Solomon, J. E. Penner-Hahn, K. O. Hodgson, E. I. Solomon, *J. Am. Chem. Soc.* **1987**, *109*, 6433–6442.
- [61] J. L. DuBois, P. Mukherjee, A. M. Collier, J. M. Mayer, E. I. Solomon, B. Hedman, T. D. P. Stack, K. O. Hodgson, *J. Am. Chem. Soc.* **1997**, *119*, 8578–8579.
- [62] S. Herres-Pawlis, P. Verma, R. Haase, P. Kang, C. T. Lyons, E. C. Wasinger, U. Flörke, G. Henkel, T. D. P. Stack, *J. Am. Chem. Soc.* **2009**, *131*, 1154–1169.
- [63] G. Y. Park, M. F. Qayyum, J. Woertink, K. O. Hodgson, B. Hedman, A. A. Narducci Sarjeant, E. I. Solomon, K. D. Karlin, *J. Am. Chem. Soc.* **2012**, *134*, 8513–8524.
- [64] A. Walli, S. Dechert, M. Bauer, S. Demeshko, F. Meyer, *Eur. J. Inorg. Chem.* **2014**, 4660–4676.
- [65] M. Bauer, H. Bertagnolli, in *Methods in Physical Chemistry*, Wiley-VCH, Weinheim, **2012**, pp. 231–269.
- [66] J. E. Bulkowski, Binucleating Ligand–Metal Complexes as Oxidation Catalysts, **1985**, US4545937A.
- [67] H.-J. Teuber, S. Benz, *Chem. Ber.* **1967**, *100*, 2077–2092.
- [68] J. N. Hamann, R. Schneider, F. Tuczek, *J. Coord. Chem.* **2015**, DOI: 10.1080/00958972.2015.1074191.

- [69] J. L. Muñoz-Muñoz, J. Berna, M. del Mar García-Molina, F. García-Molina, P. A. García-Ruiz, R. Varon, J. N. Rodríguez-Lopez, F. García-Canovas, *Biochem. Biophys. Res. Commun.* **2012**, *424*, 228–233.
- [70] J. Leonhard, B. Lygo, G. Procter, *Praxis in Der Organischen Chemie*, VCH, Weinheim, **1996**.
- [71] S. Trofimenko, J. C. Calabrese, J. S. Thompson, *Inorg. Chem.* **1987**, *26*, 1507–1514.
- [72] S. E. Howson, L. E. N. Allan, N. P. Chmel, G. J. Clarkson, R. J. Deeth, A. D. Faulkner, D. H. Simpson, P. Scott, *Dalton Trans.* **2011**, *40*, 10416–10433.
- [73] H.-D. Hardt, *Z. Anorg. Allg. Chem.* **1959**, *301*, 87–96.
- [74] A. Company, S. Palavicini, I. Garcia-Bosch, R. Mas-Ballesté, L. Que, Jr., E. V. Rybak-Akimova, L. Casella, X. Ribas, M. Costas, L. Que, Jr., *Chem. Eur. J.* **2008**, *14*, 3535–3538.
- [75] Bruker, SMART (Version 5.62), SAINT (Version 6.02), SHELXTL (Version 6.10), SADABS (Version 2.03), AXS Inc., Madison, Wisconsin, USA, **2002**.
- [76] Bruker, XPREP, Bruker AXS Inc., Madison, Wisconsin, USA, **2007**.
- [77] G. M. Sheldrick, *Acta Crystallogr. Sect. A* **1990**, *46*, 467–473.
- [78] C. B. Hübschle, G. M. Sheldrick, B. Dittrich, *J. Appl. Crystallogr.* **2011**, *44*, 1281–1284.
- [79] J. Tao, J. P. Perdew, V. N. Staroverov, G. E. Scuseria, *Phys. Rev. Lett.* **2003**, *91*, 146401-1-146401-4.
- [80] F. Weinhold, C. Landis, *Valency and Bonding - A Natural Bond Orbital Donor-Acceptor Perspective*, Cambridge University Press, New York, **2005**.
- [81] S. I. Gorelsky, *AOMix: Program for Molecular Orbital Analysis*, <http://www.sg-chem.net/>, **1997**.
- [82] S. I. Gorelsky, S. Ghosh, E. I. Solomon, *J. Am. Chem. Soc.* **2006**, *128*, 278–290.

Received: April 29, 2015

Published online on October 12, 2015